Nanoscale

Accepted Manuscript

This article can be cited before page numbers have been issued, to do this please use: M. Marín-Barba, H. Gavilán, L. Gutierrez, E. Lozano-Velasco, I. Rodriguez-Ramiro, G. Wheeler, C. J. Morris, M. P. Morales and A. Ruiz, *Nanoscale*, 2017, DOI: 10.1039/C7NR06020C.

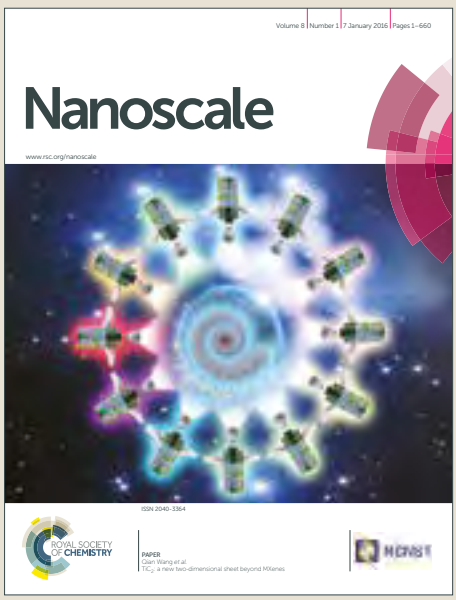

View Article Online
DOI: 10.1039/C7NR06020C

Nanoscale

ARTICLE

Unravelling the mechanisms that determine the uptake and metabolism of magnetic single and multicore nanoparticles in a *Xenopus laevis* model

Received 00th January 20xx,
Accepted 00th January 20xx

DOI: 10.1039/x0xx00000x

www.rsc.org/

M. Marín-Barba[a⊥], H. Gavilán[b⊥], L. Gutiérrez[c], E. Lozano-Velasco[a], I. Rodríguez-Ramiro[d], G. N. Wheeler[a], C. J. Morris[e], M. P. Morales[b] and A. Ruiz[e]*

Multicore superparamagnetic nanoparticles have been proposed as ideal tools for some biomedical applications because of their high magnetic moment per particle, high specific surface area and long term colloidal stability. Through controlled aggregation and packing of magnetic cores it is possible to obtain not only single-core but also multicore and hollow spheres with internal voids. In this work, we compare toxicological properties of single and multicore nanoparticles. Both types of particles showed moderate *in vitro* toxicity (MTT assay) tested in Hep G2 (human hepatocellular carcinoma) and Caco-2 (human colorectal adenocarcinoma) cells. The influence of surface chemistry in their biological behavior was also studied after functionalization with O,O'-bis(2-aminoethyl) PEG (2000 Da). For the first time, these nanoparticles were evaluated in a *Xenopus laevis* model studying their whole organism toxicity and their impact upon iron metabolism. The degree of activation of the metabolic pathway depends on the size and surface charge of the nanoparticles which determine their uptake. The results also highlight the potential of *Xenopus laevis* model bridging the gap between *in vitro* cell-based assays and rodent models for toxicity assessment to develop effective nanoparticles for biomedical applications.

Introduction

Iron oxide magnetic nanoparticles (IOMNPs) are extensively studied nowadays for their potential in biomedical applications.[1,2] Their surface chemistry can be modified, adding functionality to the material and enabling their use for gene therapy, tissue regeneration and drug delivery, to specifically target tumours using external magnetic fields[3]. Their magnetic properties can be exploited for magnetic resonance imaging and magnetic-fluid hyperthermia, which has raised hope for improved imaging techniques[4] and cancer treatment.[5,6] However, in spite of their potential, few of these biomaterials have reached clinical practice.[7]

A crucial issue for magnetic nanoparticle utilization in biomedicine and their approval by regulatory agencies depends on their biotransformation and toxicity. The course and fate of the nanoparticles once they deliver their imaging or therapeutic objective needs to be studied. Thus, the metabolism of the particles and degradation by-products must be assessed and assured. Since iron is involved in diverse cellular processes,[8] organisms display mechanisms to transport and store iron in non-toxic forms.[9] Therefore, IOMNPs are predicted to be safely incorporated into biological systems. Increasing evidence demonstrates that IOMNPs trigger iron-coping mechanisms in cells and that the degradation products of these materials are incorporated into normal iron metabolic routes.[10–16] However, nanoparticle coating has been shown to be a determinant of the IOMNPs uptake and degradation pathways.[17,18] In order to establish solid conclusions about IOMNPs toxicity and biodistribution and their cellular effects, it would be ideal to have biologically pertinent models.

Xenopus laevis is an amphibian model ideal to study the course and fate of the nanoparticles as it is an easy and flexible system in which to evaluate vertebrate embryology, basic cell and molecular biology, genomics, neurobiology and toxicology.[19] Recently, this model was used to identify the risk of exposure to contaminated water.[20] The mortality, malformations and growth inhibition of *Xenopus laevis* were studied, after challenge with metal oxide-based nanomaterial contaminants (γ-Fe_2O_3, TiO_2, ZnO and CuO). Notably, γ-Fe_2O_3 did not pose risks to amphibian populations up to 1 mg/mL where it causes developmental abnormalities. In contrast, the other nanoparticles caused gastrointestinal, spinal, and other abnormalities at concentrations of ~3 mg/L. Furthermore, it was shown that nanoparticle sizes above 200 nm had toxic effects.[21] Despite available literature on the effects of many

[a] School of Biological Sciences, University of East Anglia, Norwich Research Park, Norwich, Norfolk, NR4 7TJ, UK.
[b] Instituto de Ciencia de Materiales de Madrid, Sor Juana Inés de la Cruz 3, 28049 Madrid, Spain.
[c] Dept. Química Analítica, Instituto de Nanociencia de Aragón, Universidad de Zaragoza, 50018 Zaragoza, Spain.
[d] School of Medicine, University of East Anglia, Norwich Research Park, Norwich, Norfolk, NR4 7TJ, UK.
[e] School of Pharmacy, University of East Anglia, Norwich Research Park, Norwich, Norfolk, NR4 7TJ, UK.
⊥ These authors contributed equally to this work.
* corresponding author: G.Ruiz-Estrada@uea.ac.uk
DOI: 10.1039/x0xx00000x

View Article Online
DOI: 10.1039/C7NR06020C

compounds on the larval development of *X. laevis* in environmental studies, there are only few reports evaluating nanoparticles toxicity and biodistribution designed for biomedical applications,[22,23] and there is still a lack of knowledge bridging biotransformation studies in cell-based assays with data generated from rodent *in vivo* systems.

In this work, we report the effect of γ-Fe_2O_3 magnetic single and multicore nanoparticles suitable for bioapplications in *X. laevis* embryos. The particles have uniform size in the nanoscale and are coated with biocompatible shells. IOMNPs colloids used in this work can be classified as single-core (with only one magnetic core per particle) and multicore (with several magnetic cores per particle).[24] Single-core superparamagnetic nanoparticles have been proposed as ideal tools in biomedicine, since they display longer circulation times post-injection.[25] Indeed, this may favour their uptake in leaky vasculature regions such as tumors.[26] In contrast, for some medical applications, such as bioseparation or magnetic fluid hyperthermia, it can be advantageous to use larger multicore particles that have a large magnetic moment per particle.[27] Few *in vitro* and *in vivo* studies have been dedicated to the comparison of single-core and multicore nanoparticles[28] and there is a lack of knowledge still on how the aggregation of magnetic cores forming multicore nanoparticles affects the nanoparticle uptake and degradation.

Here we report for the first-time toxicity and metabolization of single-core and multicore nanoparticles using a combination of *in vitro* cell culture models and an *in vivo X. laevis* embryo model. The application of AC magnetic susceptibility measurements has proven to be an excellent tool to study magnetic nanoparticles in complex matrices, since the diamagnetic signal coming from tissues does not interfere with the superparamagnetic signal of the NPs.[29] This way it was possible to follow the signal of the magnetic nanoparticles in animal models[30–32] and to quantify the iron content. This is one of the greatest challenges in the nanomaterials area nowadays, *i.e.* determining how best to characterize nanoparticles and follow their transformation/degradation.[33] The study of *in vivo* fate of IOMNPs is imperative to develop successful biomedical applications. In this paper, we present for the first time, a study, by means of AC magnetic susceptibility measurements, of the intake of iron-containing particles in *X. laevis* embryos.

Results and discussion

Nanoparticles synthesis and characterization

Two different types of iron oxide nanoparticles were synthesized in this work. Single core nanoparticles (SC) were obtained by thermal decomposition of the iron(III) oleate precursor in 1-octadecene (Figure 1 A, B). Particles were 13 nm (± 1 nm) in diameter, uniform in size (Figure 1 C), relatively round and well dispersed, owing to the presence of oleic acid around the particles. In a different approach, multicore nanoparticles (MC) were obtained by polyol mediated reduction of iron(III) chloride. MC are composed of spherical 142 nm (± 23 nm) nanoparticles with a well-defined size and shape (Figure 1 D, F). These MC nanoparticles consist of smaller cores of approximately 10 nm. HRTEM and X-ray diffraction patterns have already been reported.[34] Particle structure and size were selected intentionally, since they are two key parameters that directly influence *in vivo* biological behavior. The size of intravenously injected nanoparticles greatly affects their *in vivo* biodistribution, *e.g.* particles from 60 to 150 nm in size are taken up by the reticuloendothelial system leading to rapid uptake in the liver and spleen in humans. Intravenously injected nanoparticles with diameters of 10-40 nm allow longer blood circulation and can cross capillary walls, and they are often phagocytosed by macrophages which traffic to lymph nodes and bone marrow.[35] However, how these parameters affect the greater picture of toxicity and biodegradability mechanisms is still poorly understood.

Iron oxide nanoparticles obtained by thermal decomposition are hydrophobic. To stabilize them in aqueous media and make them suitable for biological applications, oleic acid on the surface of the nanoparticle was removed with DMSA via ligand exchange reaction (SC-DMSA). Polyol mediated process render hydrophilic nanoparticles along with polyvinylpyrrolidone (PVP40), present in the reaction, however an extra capping agent like citric acid enhances the electrostatic repulsion and facilitates the final dispersion of the MC nanoparticles in aqueous media (MC-Cit). Hydrodynamic sizes are always higher than sizes measured by TEM, indicating the presence of the coating or some degree of agglomeration after surface modification, but both types of particles remain below 200 nm (34 and 181 nm were obtained for SC-DMSA and MC-Cit, respectively), an important requirement for biomedical applications. Both particles have high negative surface charge at pH 7 (Z-potential equal to -38 and -25 mV for SC-DMSA and MC-Cit, respectively). In order to evaluate the influence of the surface charge in particle absorption and biodegradation, we conjugated covalently a diamine PEG derivative to the carboxylic groups (from both DMSA and citric acid) to the surface of the nanoparticles. After PEG conjugation, average hydrodynamic size at pH 7 increased from 34 to 65 nm and from 181 to 183 nm for SC-DMSA and MC-Cit, respectively (SC-DMSA-PEG and MC-Cit-PEG) and net surface charge decreased from approximately -38 to -24 mV for SC-DMSA-PEG samples and from -25 to -18 mV for MC-Cit-PEG. Colloidal properties of aqueous suspensions of the nanoparticles at pH 7 are summarized in Table 1. Also, hydrodynamic sizes of the particles have been studied in different biological media (Figure 1S).

View Article Online
DOI: 10.1039/C7NR06020C

Table 1. Colloidal properties of aqueous suspensions of the nanoparticles at pH 7. Hydrodynamic sizes, PDI (= standard deviation/mean size) and surface charge of single and multicore nanoparticles after PEG conjugation

Sample	Hydrodynamic size (nm)	PDI	ζ-Potential (mV)
SC-DMSA	34	0.054	-38 ± 12
SC-DMSA-PEG	65	0.084	-24 ± 7
MC-Cit	181	0.201	-25 ± 9
MC-Cit-PEG	183	0.225	-18 ± 9

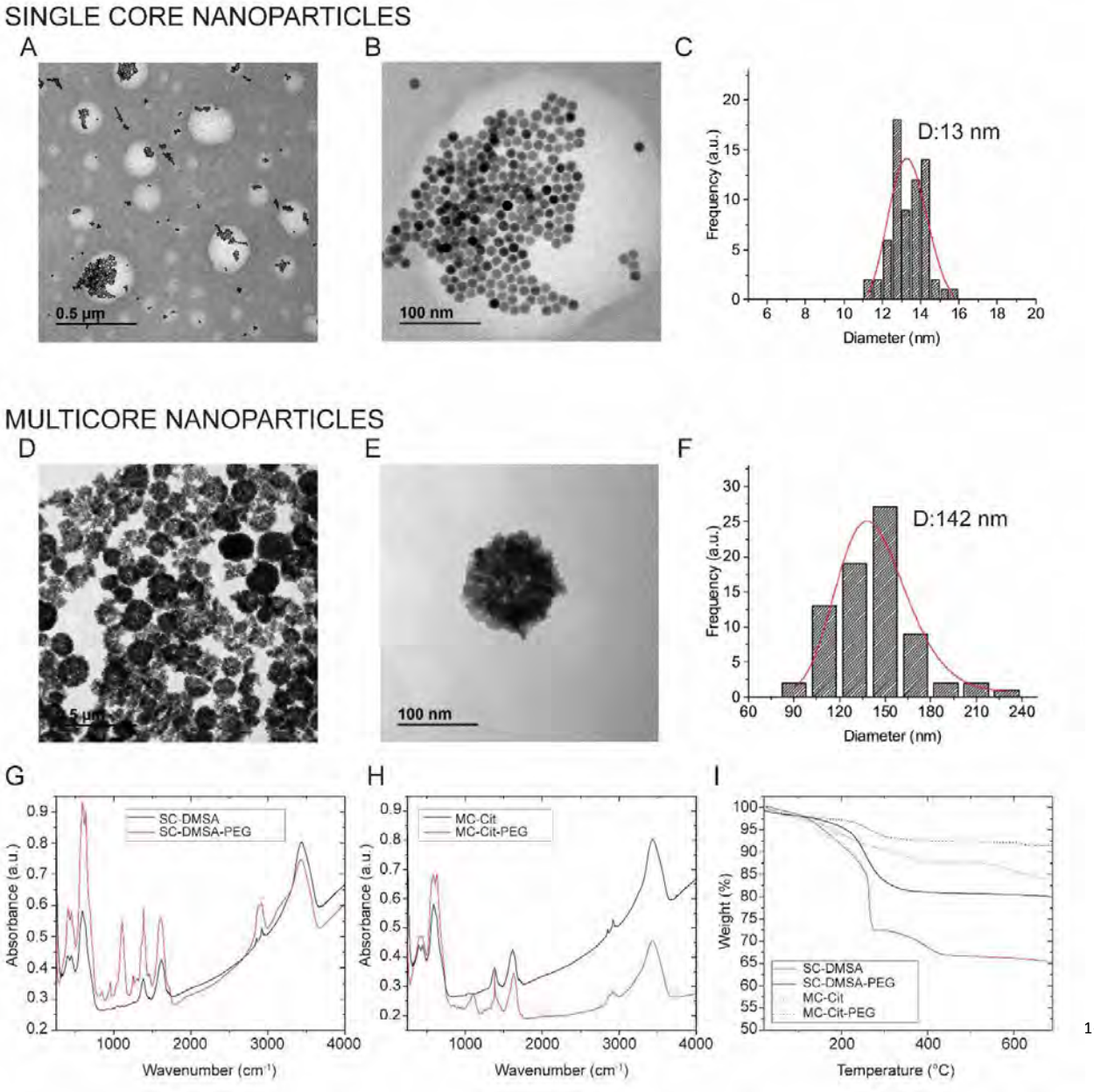

View Article Online
DOI: 10.1039/C7NR06020C

Figure 1. Transmission electron microscopy (TEM) images of single and multicore nanoparticles. (A, B) SC-DMSA. (D, E) MC-Cit. (C, F) Size distribution histograms. Red lines indicate the log-normal fitting function of TEM particle size data. Physical chemical characterization of the nanoparticles after conjugation with PEG. FTIR spectra of (G) Single-core nanoparticles. (H) Multicore nanoparticles. (I) Thermogravimetric analysis of four formulations

Nanoparticle surface modification was also confirmed by FTIR (Figure 1 G, H). For all the samples, the typical bands of metal skeleton vibration (Fe-O) in the region of 550-600 cm^{-1} and a broad peak between 3000 and 3500 cm-1 due to surface -OH groups are observed. After PEG conjugation, some peaks appeared at 1354 and 1102 cm^{-1}, indicating asymmetric and symmetric stretching of C-O-C, and out-of-plane bending of the -CH of the PEG chains at 956 cm^{-1}. TGA of the unconjugated nanoparticles reveals a weight loss of ~15 % and 8 % for SC-DMSA and MC-CIT respectively, due to the removal of physical and chemical water and capping molecules (DMSA or citric acid) (Figure 1 I). Particles modified with diamine PEG nonetheless showed a larger amount of conjugated polymer (~20 % in the case of SC-DMSA-PEG and 13 % for MC-Cit-PEG) which indicates greater reaction efficiency. In the case of SC-DMSA-PEG, the presence of ~2 molecules of PEG per nm^2 was calculated. In the case of MC-Cit-PEG is not possible to make an accurate calculation of the number of PEG molecules bounded to the surface because is not a homogeneous spherical surface due to their multicore structure. A notable decrease in the surface charge of the particles is observed after PEG conjugation, however not all carboxyl groups are modified during the reaction. The surface is not saturated probably due to the steric hindrance caused by the PEG chains, and therefore we have a limited balance of the negative surface charge coming from the DMSA or citric acid.

Toxicity *in vitro*

In vitro toxicological characterization of the nanoparticles was evaluated through the degree of cell survival by means of the standard MTT assay. The cell lines used, Hep G2 and Caco-2, represent the liver and the intestine, which are two important target organs to encounter the NPs after oral exposure or intravenous injection in a biomedical application. The analysis of cytotoxicity after incubation with the nanoparticles showed that viability of cell culture is not significantly reduced by the presence of the nanoparticles up to 160 µg/mL Fe concentration after 24 h of treatment (80-100% viability compared with the control) (Figure 2 A, B). At iron concentrations of 320 µg/mL, SC decreased the viability of both cell lines down to values of 20 %. In the case of MC, viability percentage of both cell lines is in the range of 60-80 %, indicating lower toxicity even at high iron concentrations. The effect of PEG coating is not very clear at high iron concentration. In the case of Hep G2 cells, PEG functionalization improved the cytotoxicity for SC while in Caco-2 it had no effect. For MC, PEG functionalization reduces the viability to 60 % in Caco-2 cells (Figure 2 A, B). Even though

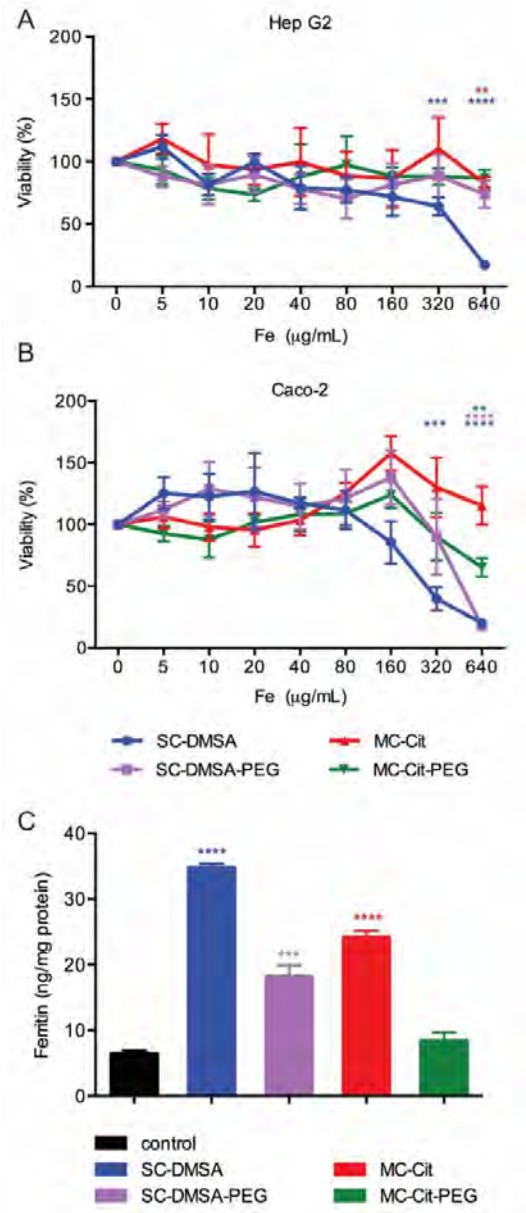

Figure 2. Evaluation of cell viability by MTT assay. (A) Hep G2 cells. (B) Caco-2 cells. Cells were treated with the nanoparticles for 24 h. (C) Ferritin formation measured by ELISA in Caco-2 cells exposed to 40 µg/mL of single or multicore nanoparticles. Data represent means ± SD (n = 3). * shows statistically-significance compared with the control (t test, *p<0.05, ** p<0.01, ***p<0.001, ****p<0.0001).

View Article Online
DOI: 10.1039/C7NR06020C

this method needs further refinement and standardization for toxicity evaluation of nanomaterials, it offers a quick, inexpensive and high-throughput methodology to perform *in vitro* cytotoxicity screens.[36]

In order to characterize the absorption and biotransformation of the nanoparticles, we determined by ELISA the ferritin formation in Caco-2 cells as a measure of iron uptake (Figure 2 C). Single core nanoparticles seem to be internalized by the cells more efficiently than multicore nanoparticles as evidenced by a 5.4-fold increase in intracellular ferritin (*cf.* control) compared with a 3.7-fold increase for MC-Cit probably due to the smaller size of the SC. PEGylated MC particles failed to alter ($p>0.05$) the ferritin levels in Caco-2 cells. The surface modification with PEG in both types of nanoparticles reduces the internalization by the cells. The coating with short-chain PEG molecules of iron oxide nanoparticles was found to shield their surface charge and decreases their internalization.[37]

In vivo evaluation of nanoparticles

To characterize the general toxicity of the nanoparticles, embryos were treated with four different concentrations, 0.25, 0.5, 0.75 and 1 mg/mL. In these experiments, nanoparticles were added at stage 38 and survival was evaluated every 24 h until embryos reach stage 45, after approximately 72 h of exposure. None of the conditions was found lethal for the embryos, therefore we decided to perform the rest of the experiments comparing a low and a high dose of nanoparticles (0.5 and 1 mg/mL). The use of the *Xenopus* model has advantages with respect to other animal models. First, embryos develop externally, allowing experiments to be performed prior to, or directly following fertilization. Also, they have a rapid embryo growth and development. A larval tadpole has a fully functional set of organs, and it can be examined to determine if any experimental intervention (in this case a solution containing nanoparticles) has had an effect.

Tadpoles treated with SC-DMSA and MC-Cit at 1 mg/mL displayed some general body toxicity compared with the control, characterized by defects in embryo body shape like bent spine or enlarged ventral fin (Figure 3 B). In the case of SC-DMSA, 20 % of the animals showed enlarged ventral fin and MC-Cit provokes a significant increase (27 %) of embryos with bent spine.

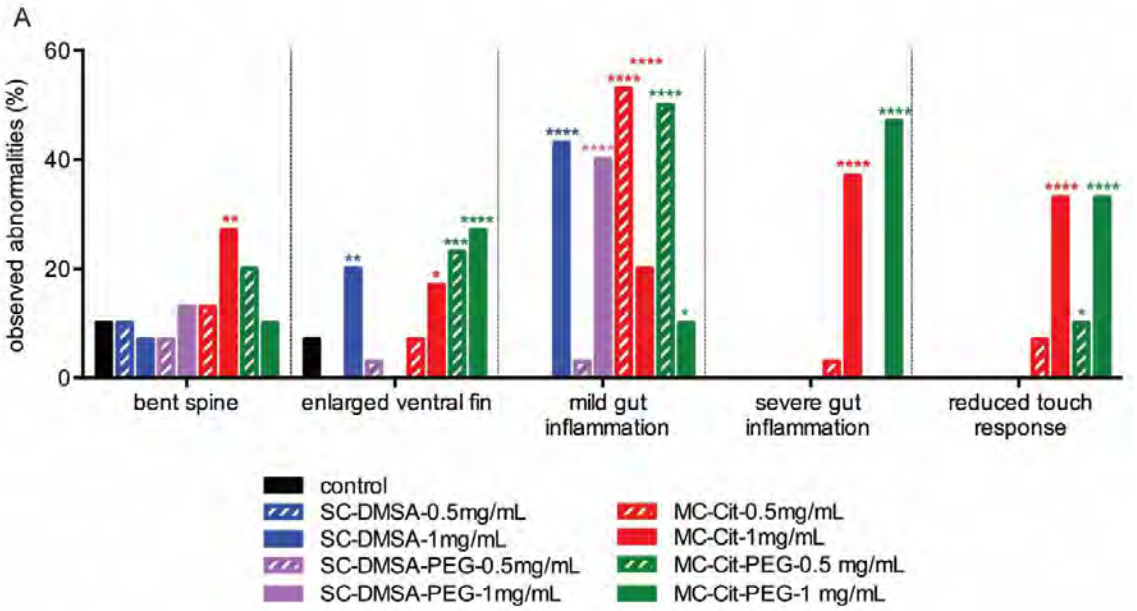

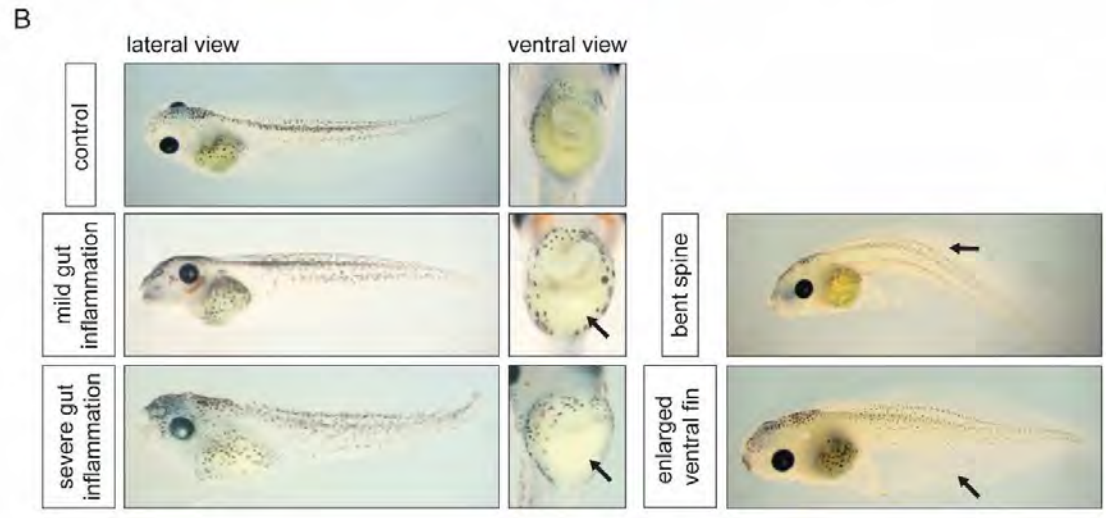

View Article Online
DOI: 10.1039/C7NR06020C

Figure 3. *Xenopus laevis* phenotypic nanotoxicity assay after 72 h of exposure from stage 38-45. (A) Quantification of embryonic abnormalities. Histograms shown are of 30 embryos per group (Chi-Square test, (*p<0.05, ** p<0.01, ***p<0.001, ****p<0.0001). (B) Representative images from the *X. laevis* phenotypic nanotoxicity assay.

Interestingly, the effect of the PEG coating for each type of NPs reduced the toxicological effect as evidenced in a 2.6-fold decrease of embryos with bent spine and a 2-fold decrease of mild gut inflammation for MC; and a significant reduction in the enlarged ventral fin phenotype for SC treated tadpoles (Figure 3 A). In the case of embryos treated with 0.5 mg/mL, defects were subtler. These results suggested a dose-dependent uptake of the NPs by the embryos. We next evaluated gut morphology as it is the main organ involved in NPs' absorption after oral ingestion. Different degrees of inflammation were observed according to the dose of the nanoparticles, but also according to their chemical structure. Mild inflammation is observed in 43 % of animals treated with SC-DMSA at 1 mg/mL. The intestine coiled structure is preserved although it is visibly enlarged. Embryos treated with MC-Cit at the same dose showed more drastic effects (20 % mild and 36 % severe inflammation). In the case of severe inflammation, the gut is not maintained or not well formed, as we are unable to see the intestinal loops. Regarding the effects on inflammation we didn't observed significant differences in PEGylated particles compared with the uncoated ones. In addition, 30 % of the animals treated with MC showed a significant decrease of touch response after 72 hours of exposure (Figure 3 A).

Electron microscopy analysis of pharynx sections (Figure 4), taken from different embryos, affords the localization of the ingested particles. The presence of the NPs in the tissue sample is evidenced by the Energy Dispersive X-ray (EDS) elemental mapping which delivers spots with brighter contrast in areas of NP accumulation, due to the higher Z atomic number of iron. NP intake is visibly detected in the images of pharynx sections of the embryos because the EDS spectra clearly showed K electron shell (K-α and K-β lines) of iron, whereas in the case of control these peaks are absent (Figure 4). EDS analysis confirmed that only at the dose of 1 mg/mL, SC-DMSA and MC-Cit, could be detected in the upper body tissue sections, in contrast with the control. PEGylated nanoparticles (SC or MC) were undetectable in all organisms. We also observed SC-DMSA in the gills of the embryos (Figure 2S). These results agree with the size-dependent deposition in the intestine and/or the gills in Zebrafish observed for silver nanoparticles. Particles from 10-20 nm showed increased bioavailability compared with 140 nm particles.[38] In our case, the deposition of SC-DMSA in the gills is directly related to the smaller size and larger surface area compared with MC-Cit, providing increased adherence, penetration, and deposition in the organism.

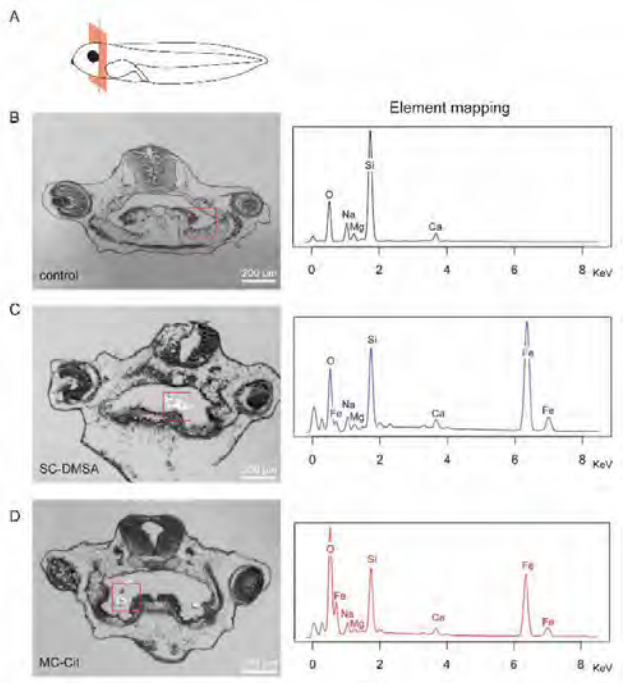

Figure 4. Scanning electron microscopy (SEM) images of pharynx sections from different embryos. (A) Schematic representation of the transversal section analyzed. (B) Control. (C) Embryos exposed to SC-DMSA nanoparticles (1 mg/mL, 72 h). (D) Embryos exposed to MC-Cit nanoparticles (1 mg/mL, 72 h). Right panel shows elemental analysis of red selected areas in the images obtained by Energy Dispersive X-ray Spectrometry (SEM-EDS).

Iron quantification. AC magnetic susceptibility and ICP-OES

In order to quantify the iron present in the samples through SEM-EDS analysis, the application of quantitative correction procedures is needed, which are sometimes referred to as matrix corrections.[39] As SEM only provides local information, the quantitative analysis of NP intake, was performed through magnetic characterization of freeze-dried tissue samples and iron elemental analysis of acid digested embryos. Moreover, these techniques allow the comparison of the accumulation depending on the coating and the surface charge (DMSA, citric acid, and PEG functionalization).

In order to evaluate the accumulation of the nanoparticles in the animals, we performed AC susceptibility of pools of seven animals. Magnetic measurements, especially AC magnetic susceptibility, are extremely sensitive being able to distinguish the contribution from the magnetic nanoparticles from that of

View Article Online
DOI: 10.1039/C7NR06020C
Journal Name ARTICLE

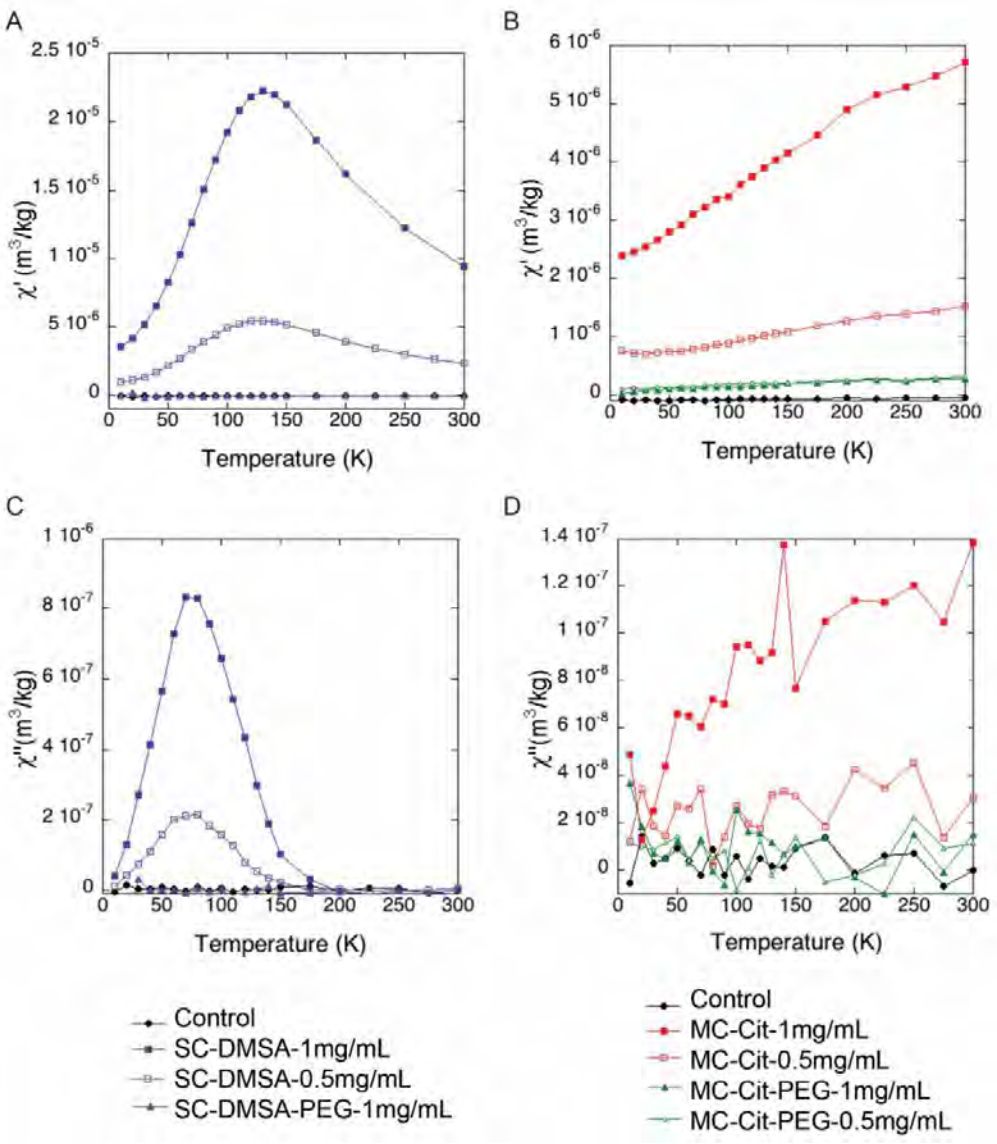

Figure 5. AC magnetic susceptibility measurement of embryo tissue samples. In-phase (χ'(T)) and out-of-phase (χ''(T)) components of the magnetic susceptibility, per mass of sample, corresponding to freeze-dried tissues from different embryos after exposure (72 h): (A, C) Embryos exposed to SC. (B, D) Embryos exposed to MC. (n = 7 per group).

other endogenous iron-containing species, usually present in a bigger concentration but with weaker magnetic signal than the nanoparticles. The presence of magnetic nanoparticles can be identified by a maximum in the in-phase magnetic susceptibility (χ') accompanied by a maximum at slightly lower temperatures in the out-of-phase susceptibility (χ''). The temperature location of the maxima depends on the nanoparticle (material, size, aggregation degree, etc.). The height of the maxima is a surrogate measurement of the concentration of nanoparticles.

In our case, a dose-dependent amount of nanoparticles is observed in the animals treated with particles without PEG coating (Figure 5), independently if they are SC or MC. Interestingly PEG coated nanoparticles, both SC and MC, were below the detection limits of the technique. These results are in agreement with what we observed by SEM-EDS. In this work, the presence of ferritin, the iron storage protein with an out-of-phase susceptibility maxima located at around 10 K,[18] has not been observed. The absence of a substantial paramagnetic contribution, usually observed at the lowest temperatures, indicates that the concentration of free iron atoms is very low, indicating that NP degradation process is limited if not absent in the timescale of these experiments.

Through AC magnetic susceptibility measurements, dose-dependent amounts of nanoparticles (SC-DMSA and MC-Cit)

View Article Online
DOI: 10.1039/C7NR06020C

were detected. In addition, a quantitative analysis of NP intake was performed by ICP-OES (Figure 6). Elemental analysis results evidenced a dose-dependent iron absorption, which is in agreement with the iron content detected by AC magnetic susceptibility. The absorption of SC-DMSA detected in the embryos has been confirmed by ICP-OES, a three or five-fold increase in comparison with MC-Cit for iron concentrations of 0.5 and 1 mg/mL, respectively. Interestingly, the iron content in the animals treated with PEGylated NPs is comparable to the control indicating a very low absorption of these NPs.

One possible explanation for the visual disturbance of the intestine structure of the embryos treated with MC-Cit-PEG, could be that the particles are rapidly excreted by the organism and therefore the iron content in these animals is seen as low. As we previously observed in Caco-2 cells, PEG functionalization reduces net surface charge of the particles and this effect could reduce the absorption of the particles in the gut favouring their excretion. Surface functionalization with PEG has been reported to enable particles to diffuse through mucus in the gastrointestinal tract at a rate similar to diffusion through water. It has been hypothesized that this occurs by reduction of particle-mucus interactions.[40] There is also evidence that PEG-coating can decrease macrophage or HeLa uptake of iron particles where the polymer increases uptake hindrance compared with uncoated NPs.[41] Another possible explanation for the morphological alterations observed at higher doses of nanoparticles could be the presence of polyol used during the MC synthesis. Other studies have shown that polyol-made nanoparticles produce *in vitro* (10 µg/mL) and *in vivo* (0.8 mg/kg) toxicity.[42]

Iron metabolism

Since iron resulting from NP degradation is predicted to be processed by iron metabolic pathways, we next studied the expression of different genes involved in iron metabolism and oxidative stress. The expression of genes linked to both processes was assessed by real-time quantitative PCR (RT-qPCR) in embryos treated with SC-DMSA and MC-Cit after 72 h of treatment with the nanoparticles at 1 mg/mL, taking into account that only at highest doses could we detect a significant amount of absorbed nanoparticles (Figure 7 A).

In the case of SC-DMSA treated embryos, *transferrin* and *dmt1* increased 2.6 and 2-fold respectively (cf. control) coupled with a 70 % downregulation of *hepcidin*. In contrast, the MC-Cit treated embryos displayed marginal increases ($p<0.05$) in *hepcidin*, and *transferrin* and *dmt1* levels remained unchanged. In both cases the transcription of *ferritin* is increased after nanoparticle treatment, 2.9-fold change for SC-DMSA and 1.9-fold change for MC-Cit treated embryos Figure 7 A).

From these data, we can describe differences in the metabolic activation pathway of single-core or multicore nanoparticles. After iron ingestion, ferrous ions (Fe^{2+}) are absorbed in the enterocytes through the divalent metal transporter-1 (DMT1). In the apical membrane of the enterocytes, the cytochrome B facilitates the reduction of ferric to ferrous ions enabling the absorption of iron.

In the basolateral membrane of the enterocytes the ferroportin transporter is located together with hephaestin which oxidize ferrous ions and allows transferrin to bind iron and carry it in the bloodstream through the different organs. Hepcidin negatively regulates the entry of iron into circulation through inhibiting ferroportin in case of iron overload (Figure 8 A). Ferritin is the most important protein involved in iron storage within cells, and the levels of Fe^{2+} present in the organism regulates its expression.[43]

From magnetic measurements and elemental analysis, we detected a higher absorption of SC-DMSA compared with MC-Cit. We propose that the rate of particle internalization into the embryos will dictate the time at which iron metabolic pathway activation is measurable. In the case of SC-DMSA treated embryos, *dmt-1*, *transferrin* and *ferritin* have the highest levels of transcription. The increase in ferritin in embryos treated with SC-DMSA compared with MC-Cit, follows the same pattern observed in Caco-2 cells where the protein was detected by ELISA suggesting a higher iron bioavailability from single-core nanoparticles. *Hepcidin* is downregulated for SC-DMSA, which implies a saturation of the metabolic pathway of iron. In the case of MC-Cit only *ferritin* and *hepcidin* are upregulated corroborating a slower activation of the iron metabolic pathway depending on the amount of internalized particles after 72 h of treatment.

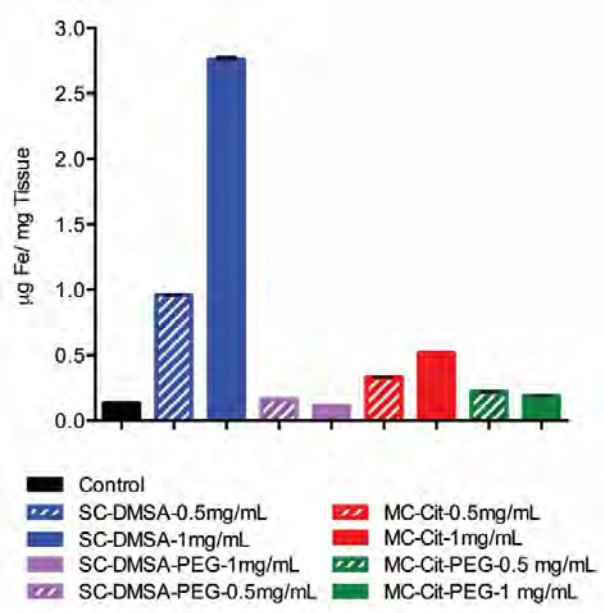

Figure 6. Iron quantification though ICP-OES of acid digested tissues from embryos treated at different concentrations of IOMNPs. Striped pattern: 0.5 mg/mL. Solid pattern: 1 mg/mL. (n = 7 per group).

View Article Online
DOI: 10.1039/C7NR06020C

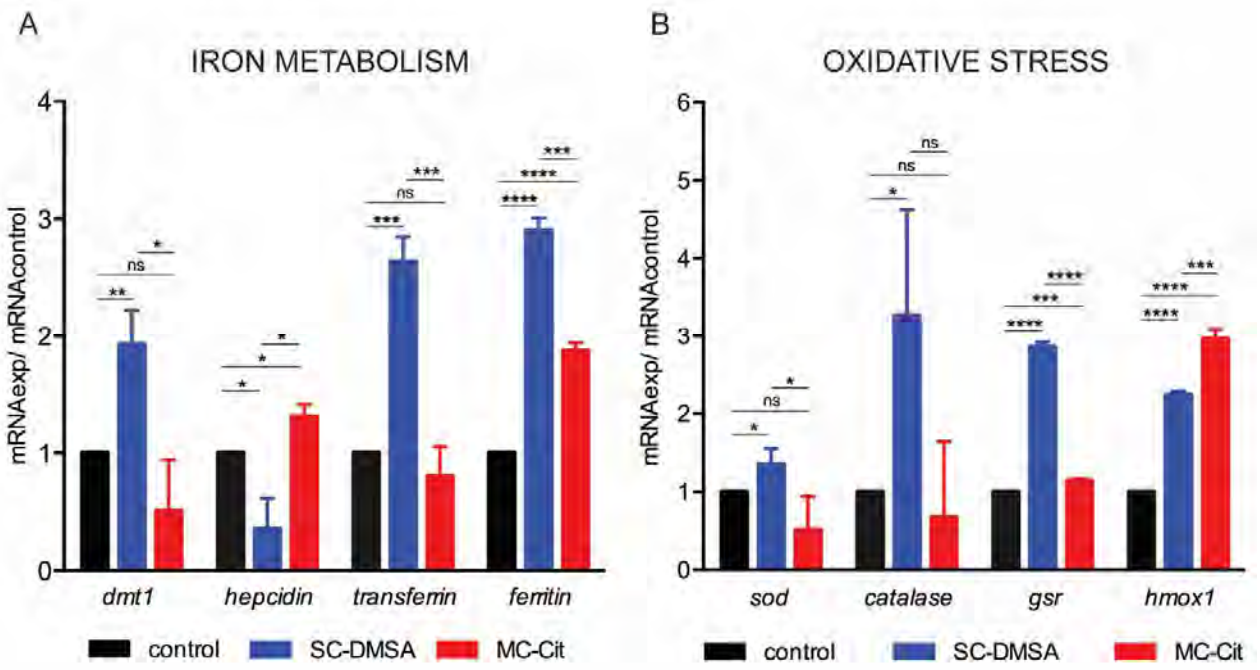

Figure 7. Effect on the expression of different genes in *X. laevis* embryos exposed to SC-DMSA or MC-Cit after 72 h at 1 mg/mL. (A) Genes involved in iron metabolism. (B) Genes involved in oxidative stress response. (n = 7 per group). * shows statistically-significance compared with the control (t test, ns >0.05, *p<0.05, ** p<0.01, ***p<0.001, ****p<0.0001).

Oxidative stress

In embryos treated with SC-DMSA or MC-Cit at 1 mg/mL we observed a 2.2 and 2.96-fold increase in hmox1 (cf. control) respectively after 72 h of exposure (Figure 7 B). Increases in transcript levels of *hmox1* have been described in macrophages treated with iron oxide hybrids nanomaterials.[44] Hmox1 is induced after oxidative stress, reactive oxygen species or heavy metals, thus degrading heme group to form biliverdin and Fe^{2+}. The production of Fe^{2+} leads to the activation of iron regulatory protein (IRP) which is able to control the translation of iron sensitive proteins such as ferritin. In the absence of iron, IRP binds to ferritin mRNA and inhibits its translation. However, when iron ions are available, they bind to IRP and release it from ferritin mRNA, thus allowing its translation (Figure 8 B).[45] The increase in Fe^{2+} in the embryos 72 h after the treatment, activates iron response proteins, which activates the translation of proteins involved in iron metabolism such as ferritin. We show *in vivo* the activation by Hmox-1 of iron regulatory proteins and their effect in the transcription of ferritin mRNA associated to the treatment with iron oxide nanoparticles (Figure 7 A, B).

Other oxidative stress response genes showed an increase in expression in the case of embryos treated with SC-DMSA (sod 1.35- fold, catalase 3.27-fold and gsr 2.85-fold) compared with MC-Cit (sod 0.5- fold, catalase 0.67-fold and gsr 1.14-fold) (Figure 7 B). These results suggest the activation of protective mechanisms depending on nanoparticle uptake in order to reduce reactive oxygen species (ROS) generated during the biodegradation process. This is the early response of the organism when nanoparticle clearance induces the formation of ROS. However, we are not in the presence of an acute state of oxidative stress when a general decrease of antioxidant enzymes takes place.[46]

With these results, we provide evidence that an early developmental vertebrate model such as *Xenopus laevis* is a rapid and inexpensive system for NP toxicity assessment, compared with adult mammalian models. Because most theranostic applications need nanoparticles to be taken up by the cells, intracellular nano-biodegradation in an *in vitro* model needs to correlate with *in vivo* observations. In the case of IONPs degradation *in vitro* and their bioavailability by the cells translated into an increase of ferritin levels (Figure 2 C), should correlate with the corresponding activation of the iron metabolic pathway as shown in Figure 7 A).

Here we demonstrated for the first time the study, by means of AC magnetic susceptibility measurements, of the intake of iron-containing particles in *X. laevis* embryos. We postulate that the rate of particle internalization into the embryos will

View Article Online
DOI: 10.1039/C7NR06020C

dictate the time at which iron metabolic pathway activation is measurable. Also, the NP deposition and uptake likely depends on the physico-chemical characteristics of the nanoparticles in terms of structure, size, and chemical modification of the surface. We can consider *Xenopus* as the bridge between cell-based assays and mammalian models taking into account that the activation of the iron metabolic pathway, especially with SC-DMSA, correlates with previous results in different murine models tracking IONPs biodegradation.[18,32,47] The significant increase of transcript levels of *ferritin* or *dmt1* correlates with previous observations in a Wistar rat animal model where these proteins were quantified by ELISA in tissue samples from the liver, spleen and kidneys, 24 hours after SC-DMSA intravenous injection.[18] Also, multicore nanoparticles degradation has been described *in vitro* recently, starting with the dissociation of the multigrain structure and following with the massive dissolution of the iron oxide cores[48]. These results highlight the necessity to study at longer times the nanoparticle biotransformation in *X. laevis*.

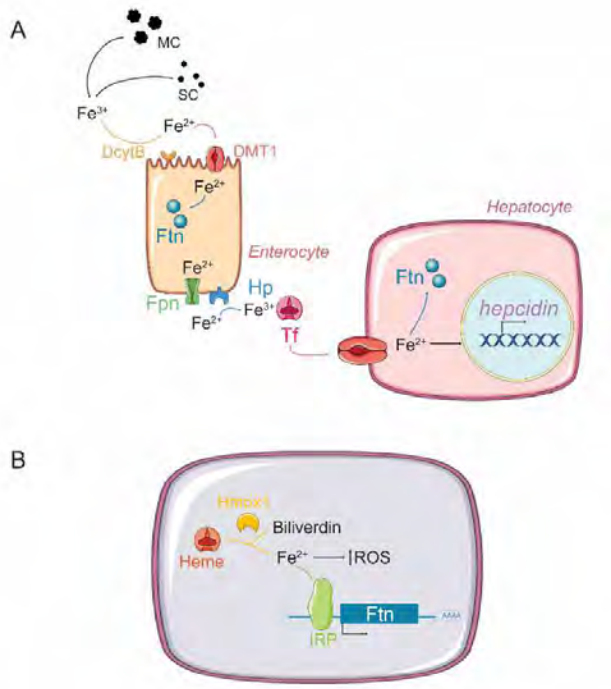

Figure 8. Schematic representation of iron metabolic pathway. (A) Enterocyte uptake and transfer of iron: Ferrous ions (Fe^{2+}) are absorbed in the enterocytes through the divalent metal transporter-1 (DMT1). In the apical membrane of the enterocytes, the cytochrome B (DcytB) facilitates the reduction of ferric to ferrous ions enabling the absorption of iron. In the basolateral membrane of the enterocytes the ferroportin transporter (Fpn) is located together with hephaestin (Hp), which oxidize ferrous ions and allows transferrin to bind iron and carry it in the bloodstream through the different organs. In the liver iron will be stored in complex with ferritin (Ftn). In the case of iron overload Hepcidin transcription is activated and it will regulate the entry of iron into circulation through inhibiting ferroportin. (B) Regulation of ferritin mRNA translation by Hmox1 and IRP: Iron overload induces ROS generation. Hmox1 is induced after oxidative stress, thus degrading heme group to form biliverdin and ferrous ions. The production of Fe^{2+} leads to the activation of iron regulatory protein (IRP) which is able to control the translation of iron sensitive proteins such as ferritin. In the absence of iron, IRP binds to ferritin mRNA and inhibits its translation. However, when iron ions are available, they bind to IRP and release it from ferritin mRNA, thus allowing its translation.

Conclusions

In this work, the toxicity and metabolization of DMSA, citric acid and PEG coated single and multicore iron oxide magnetic nanoparticles have been studied in Hep G2 and Caco-2 cell lines, and in an amphibian animal (*Xenopus laevis*) model during its embryo development. The viability of both cell lines is preserved in all cases when treated with the nanoparticles up to an iron concentration of 160 µg/mL. Above that concentration, only PEGylated nanoparticles didn't cause toxicity on Hep G2 cells but Caco-2 cells were more sensitive. In the case of the *in vivo* viability, although none of the single-core nor multicore coated nanoparticles were found lethal for the embryos, more dramatic effects were observed in the treatment with multicore nanoparticles. Single-core nanoparticles are absorbed (three or five-fold increase for doses of 0.5 and 1 mg/mL, respectively) in comparison with multicore ones suggesting size-dependent differences in the deposition an uptake of the nanoparticles. Monitoring nanoparticle biodegradation is critical for therapeutic efficiency and safety issues. Depending on their structural organization (single or multicore) and surface chemistry, the embryos will trigger the iron metabolic pathway to varying degrees. These findings advance the understanding of iron oxide nanoparticle metabolization in an early developmental vertebrate model like *Xenopus laevis*, which offers a quick, inexpensive and high-throughput alternative prior toxicity assessment of nanotherapeutics in rodent models.

Materials and Experimental Methods

Materials

Commercial products: iron(III) chloride hexahydrate, oleylamine, oleic acid, meso-2,3-dimercaptosuccinic acid (DMSA), 1-octadecene, toluene, dimethyl sulfoxide, O,O'-bis(2-aminoethyl)PEG, 2000 Da, polyvinylpyrrolidone PVP40, sodium acetate trihydrated, and citric acid (Sigma-Aldrich), sodium oleate (Riedel-de Haen), n-hexane (Scharlau), ethyl-3-(3-dimethylaminopropyl)-carbodiimide, ethylene glycol (Fluka), and ethanol (Panreac). Dialysis tubing cellulose membranes were purchased from Sigma-Aldrich and washed prior to use.

Nanoparticles synthesis

View Article Online
DOI: 10.1039/C7NR06020C

Synthesis of iron oxide single-core nanoparticles (SC). The synthesis of iron oxide nanoparticles has been based on a previous work described in the literature.[49] The reaction was carried out under nitrogen. In a round-bottomed flask (500 mL), equipped with a mechanical stirrer (glass stirrer shaft), thermometer, entry for nitrogen flow and reflux condenser, iron(III) oleate (4.54 g) was mixed with oleic acid (0.724 g) in 1-octadecene (50 mL). The mixture was stirred (100 rpm) and slowly heated (5 ºC·min^{-1} for T< 100ºC, and 2ºC·min^{-1} for T> 100ºC) until reflux (325ºC) with a heating mantle. The heating mantle was withdrawn, and the system was cooled down to room temperature. The resulting black mixture was washed with ethanol several times by centrifugation (RCF = 7500) and magnetic decantation. The resulting dried black solid was redispersed in hexane.

Synthesis of iron oxide multicore nanoparticles (MC). The synthesis of iron oxide nanoparticles has been based on a previous work described in the literature[50] but the experimental procedure and the concentration of NaAc have been varied. Typically, 2.62 mmol iron(III) chloride were dissolved with ultrasound in 109 mL of ethylene glycol. Then, 140 mmol PVP40 were added slowly under vigorously magnetic stirring (>1000 rpm) and mild heating until completely dissolved. Then, 26.2 mmol of NaAc·3H_2O were added to the solution. The mixture was sealed in a Teflon-lined autoclave (125 mL) and maintained at 200 °C for 16 h for solvothermal crystallization, following cooling inside oven. The precipitated solid product was washed with ethanol and distilled water through centrifugation (RCF = 7500) several times.

Surface modification

-Ligand exchange with dimercaptosuccinic acid on single-core NPs (SC-DMSA). For DMSA ligand exchange, a standard procedure was used.[51] In a typical experiment, ethanol (20 mL) was added to a volume of SC dispersed in hexane containing a mass of Fe_3O_4 of 50 mg. The mixture was sonicated and then placed on a magnet to separate the liquid from the black solid residue of nanoparticles. The residue was washed with more ethanol (5 x 10 mL) following the same procedure, until the discarded liquid had a clean appearance. The remaining black residue was dispersed in toluene (20 mL) and the dispersion added to a solution of DMSA (90 mg) in dimethyl sulfoxide (5 mL). The resulting black suspension was then shaken in a laboratory tube rotator. After 2 days, SC-DMSA nanoparticles were precipitated as a black powder stuck to the glass tube and the liquid phase was transparent and pale yellow. The liquid was discarded and the nanoparticles were washed with ethanol (4 x 10 mL), sonicating and centrifuging (RCF = 7500). The final black solid was air dried and redispersed in distilled water. KOH 1 M was added to increase the pH to 10 and HNO_3 0.01 M was used to lower the pH to 7. The dispersion was then placed in a cellulose membrane and dialyzed for 5 days in distilled water, to remove any excess of unreacted DMSA and any other small impurities that may be present in the dispersion without being attached to the nanoparticles.

-Surface coating with citric acid on multicore NPs (MC-Cit). For citric acid coating a standard procedure was used.[24,52] First, sample volume equivalent to 20 mg of Fe was adjusted to pH 2 and then dispersed in 13 mL of a solution of citric acid 0.1 M. Afterwards, the mixture was heated at 80 °C for 30 min. The solution was centrifuged and washed with distilled water. Finally, the pH was adjusted first to 11 with KOH 1M and then to 7 with HNO_3 0.01 M.

-Surface coating with polyethylene glycol (SC-DMSA-PEG and MC-Cit-PEG). PEG conjugation reaction has been based on a previous work described in the literature.[37] Amine-functionalized PEG was attached to SC-DMSA or MC-Cit via an ethyl-3-(3-dimethylaminopropyl)-carbodiimide (EDC)-mediated coupling reaction using the polymer O,O'-bis(2-aminoethyl)PEG, 2000 Da (Figure 3S). PEGylation reaction was carried out in a refrigerated ultrasonic bath; an aqueous solution containing 10 mg SC-DMSA or MC-Cit was mixed with the PEG derivative (4 mg). The total amount of EDC (1 mg) was divided into five aliquots, one of which was added every 1 h, and the fifth 4 h after the previous addition. The molar ratio of COOH groups/amine groups/EDC was 1:1.5:1; pH was adjusted to 6, and the mixture was sonicated (4 h, 25 °C), followed by extensive dialysis.

Nanoparticle structural characterization

The particle sizes and morphologies were determined by transmission electron microscopy (TEM) with a JEM1010 microscope (JEOL, Peabody, USA) operating at 100 kV. Samples were prepared by placing a drop of the uncoated particles suspended in water onto a carbon coated copper grid and allowing it to dry at room temperature. The size distributions were determined by manual measurement of more than 100 particles using the public domain software ImageJ. The presence of the coating and the washing process was also confirmed and studied by Fourier transform infrared spectroscopy (FTIR) in the range of 4000-250 cm^{-1} by use of a Bruker (USA) IFS 66VS. The samples for FTIR were prepared diluting the dried powder in KBr at 2 % by weight and pressing it into a pellet. The presence of the coating was also studied by thermogravimetric analyses (TGA). They were performed in a Seiko TG/DTA 320U thermobalance, whose temperature scanning range is from room temperature up to 900 °C. For this work, samples were heated from room temperature to 700 °C at 10 °C/min under an air flow of 100 mL·min^{-1}. Platinum pans were used and α-Al_2O_3 was used as reference. Colloidal properties were studied in a Zetasizer Nano S, from Malvern Instruments (UK). The hydrodynamic size was determined by Dynamic Light Scattering (DLS) and the zeta potential was measured as a function of pH at 25 °C, using HNO_3 and KOH to change the pH of the suspensions. Hydrodynamic size is given as the intensity-weighted mean.

Cell culture

Caco-2 cells (HTB-37) and HepG2 (HB-8065) were obtained from American Type Culture Collection (Manassas, VA, USA) and stored in liquid nitrogen. Hep G2 (human hepatocellular

View Article Online
DOI: 10.1039/C7NR06020C

carcinoma) and Caco-2 (human colorectal adenocarcinoma) cells were cultured as mono-layers in Dulbecco's modified Eagle medium supplemented with 2% penicillin-streptomycin and 10 % fetal bovine serum, in a humidified incubator (37 °C, 5% CO2). For toxicity experiments, cells were seeded in 96-well plates (approximately 1 x 10^4 cells/well, 200 µL/well). For iron uptake experiments, Caco-2 cells between passages 30-36 were seeded onto collagen-coated 12-well plates (Bio-Greiner, UK) at a density of 2 x 10^5 cells/well suspended in 1 mL of supplemented DMEM which was replaced every 2 days. Cells were used on confluence at days 13-15 post-seeding. In order to ensure a low basal media iron levels, 24 hours prior to the initiation of the nanoparticles treatments, the DMEM medium was replaced by Eagle's minimum essential medium (MEM) without foetal bovine serum supplemented with 10 mmol/L PIPES [piperazine-N, N' –bis-(2-ethanesulfonic acid)], 26.1 mM $NaHCO_3$, 19.4 mmol/L glucose, 1 % antibiotic-antimycotic solution, 11 µmol/L hydrocortisone, 0.87 µmol/L insulin, 0.02 µmol/L sodium selenite (Na_2SeO_3), 0.05 µmol/L triiodothyronine and 20 µg/L epidermal growth factor.[53] The day of the experiment, the nanoparticles were diluted in the low-iron MEM to obtain a 40 µg/mL final iron concentration and subsequently Caco-2 cells were exposed for 24 hours with the treatments. Ferritin formation was measured 24 h after treatment. Cells were rinsed with Milli-Q (18.2 MΩ) H_2O and subsequently lysed by scraping in 100 µL (12-well plates) of CelLytic M (Sigma-Aldrich, Gillingham, UK). Cell lysates were kept on ice for 15 min and stored at −80 ◦C. For analysis, samples were thawed and centrifuged at 14,000× g for 15 min. Cellular debris was discarded and the supernatant containing the proteins was analysed for ferritin using the Spectro Ferritin ELISA assay (Ramco Laboratories Inc., Stafford, TX, USA). The ferritin concentration in the samples was determined using a microplate reader at an excitation wavelength of 500 nm according to the manufacturer's protocol. Ferritin concentrations were normalized to total cell protein using the Pierce Protein BCA protein assay (ThermoFisher Scientific, Loughborough, UK).

Cytotoxicity assay (MTT)

Cell viability was determined using the standard 3-(4,5-dimethylthiazol-2-yl)-2,5-diphenyl tetrazolium bromide (MTT) assay 24 h after exposure to NP. Cells were seeded in 96-well plates at (approximately 1 x 10^4 cells/well, 200 µL/well). In total 60 wells were seeded per plate (6 rows x 10 columns) as the outer wells were left empty to avoid errors due to evaporation. Each row was used as a replicate (3 wells/condition) and serial dilutions went across the columns of the plate. Cells were left to grow until 70-80 % confluency. NP-containing medium was removed after 24 h, cells were rinsed three times with PBS, and MTT solution in medium (final MTT concentration 50 µg/mL) was added and incubated (2 h, 37 °C). The MTT solution was removed without disturbing cells, 0.2 mL/well of DMSO and 0.025 mL/well of Sorensen buffer were added, the plates were shaken gently to dissolve formazan crystals, and the absorbance was read on a microplate reader at 550 nm. Cell viability (%) was calculated as [(A − B)/A × 100], where A and B are the absorbance of control and treated cells, respectively. Values represent mean ± SD (n = 3).

***In vivo* test**

All experiments were performed in compliance with the relevant laws and institutional guidelines at the University of East Anglia. The research has been approved by the local ethical review committee according to UK Home Office regulations. *Xenopus laevis* embryo toxicity assays were carried out as described before[54,55]. Briefly, adult females were primed with PMSG (Pregnant Mare's Serum Gonadotropin) and induced with Chorulon. Eggs were obtained manually and fertilized in a petri dish by adding male sperm (male testis incubated with 2mL 1 x MMR (Marc's modified ringers) + 8 mL FBS). The fertilized embryos were dejellied *via* cysteine, and the embryos were plated in BSA-coated petri dishes covered with 0.1 x MMR. Embryos were left at 23 ºC until they reached stage 38, and then plated in 24-well plates (7 embryos/well) in 0.1 x MMR medium containing the nanoparticles and incubated at 23 ºC. Non-treated embryos were used as control. The mortality and the morphological changes of the embryos were recorded every 24 h until embryos reached stage 45.

Histological evaluation

When the embryos reached the appropriate stage, they were fixed in MEMFA (3.7 % Formaldehyde, 1X MEM salts and DEPC H2O) overnight at 4ºC. Samples were washed in PBS, dehydrated and kept in 100% ethanol. To embed embryos in wax, they were directly washed in a 65 ºC oven first in histoclear, then in 1:1 histoclear:wax and finally wax 30 min to 1 h each wash. Then the embryos were and placed in molds with wax. Embryos were sectioned using a microtome generating 10 µm slices. Slices were then hydrated in water and dried to be analyzed by Scanning electron microscopy.

Magnetic characterization

The resulting freeze-dried samples were placed into gelatin capsules for their magnetic characterization in a Quantum Design MPMS-XL SQUID magnetometer with an AC susceptibility option. The measurements were performed with AC amplitude of 0.41 Oe, in the temperature range between 1.8 and 300 K and at a frequency of 11 Hz.

Iron content analysis

Groups of 7 embryos were pooled. Animals were weighed and lyophilized 72 hours in a Telstar lyoquest lyophilizer, and the iron content was measured by Inductively Coupled Plasma-Optical Emission Spectrometry (ICP-OES) in an Optima 2100 DV from PerkinElmer, after acid digestion, with concentrated HNO_3 during 1 h; or kept freeze-dried for magnetic characterization, respectively. The sample manipulation was

View Article Online
DOI: 10.1039/C7NR06020C

performed using disposable plastic material to avoid ferromagnetic contamination.

RNA extraction and quantitative PCR

Groups of 7 embryos were snap frozen in liquid nitrogen. RNA was extracted using High Pure RNA isolation kit (Roche) and 1 µg of RNA was taken to synthetize cDNA using Maxima First Strand cDNA synthesis kit (Thermofisher). RT-PCR was performed using SYBER Green detection method. Primers were designed targeting both copies of *X. laevis* genes. Gapdh have been used as a control.

Primers	Sequence 5'-3'
fth1_F	tggagtaacaccctggaagc
fth1_R	aggatcaaccttgtcggatg
tf_F	agaaagggcaagtgggtttt
tf_R	tctggcaaagtgacaacagc
dmt1_F	cagaggatgaaacgcactca
dmt1_R	atcctgccactgatccagac
hepcidin_F	aaatcaaccccaatctgctg
hepcidin_R	gtttgttgattgccgaaggt
hmox1_F	ggagacctctcaggtggaca
hmox1_R	atggagttcatacgggaacg
sod2_F	tgtgcaggctcagtgtttgt
sod2_R	gctgcagagcaccataatca
gsr_F	gcaaagaggagaaggtggtg
gsr_R	cggaggaagtcggatgaata
cat1_F	cttctgcccagatgcttttc
cat1_R	agttgcccagagcgacttta
gapdh_F	ctttgatgctgatgctggaa
gapdh_R	gaagaggggttgacaggtga

Conflicts of interest

There are no conflicts to declare.

Acknowledgements

M. Marín-Barba has been supported by the People Program (Marie Curie Actions) of the European Union's Seventh Framework Program FP7 under REA grant agreement number 607142 (DevCom). This work was supported by 7-People Framework – Marie Curie Industry and Academia Partnerships & Pathways scheme (DNA-TRAP project, grant agreement nr. 612338), the European Commission Framework Program 7 (NanoMag project, NO 604448) and by the Spanish Ministry of Economy and Competitiveness (Mago project, No. MAT2014-52069-R). H. Gavilán has carried out this work while undertaking a doctoral program on Advanced Chemistry at the Complutense University of Madrid. L. Gutiérrez acknowledges financial support from the Ramón y Cajal subprogram (RYC-2014-15512). E. Lozano-Velasco acknowledges support from Marie Curie fellowship (705089-MIR-CHROM-C). FTIR spectroscopy and thermogravimetric and chemical analysis were carried out in the support laboratories of Instituto de Ciencia de Materiales de Madrid (ICMM/CSIC). Authors acknowledge the facilities and the scientific and technical assistance, especially that of Bertrand Leze from the SEM service of the University of East Anglia.

References

1 Roger, J.; Pons, J. N.; Massart, R.; Halbreich, A.; Bacri, J. C. Some Biomedical Applications of Ferrofluids. *Eur Phys J AP* 1999, **5**, 321-325.
2 Schutt, W.; Gruttner, C.; Hafeli, U.; Zborowski, M.; Teller, J.; Putzar, H.; Schumichen, C. Applications of Magnetic Targeting in Diagnosis and Therapy-Possibilities and Limitations: A Mini-Review. *Hybridoma* 1997, **16**, 109-117.
3 Mejias, R.; Perez-Yague, S.; Gutierrez, L.; Cabrera, L. I.; Spada, R.; Acedo, P.; Serna, C. J.; Lazaro, F. J.; Villanueva, A.; Morales Mdel, P.; et al. Dimercaptosuccinic Acid-Coated Magnetite Nanoparticles for Magnetically Guided in Vivo Delivery of Interferon Gamma for Cancer Immunotherapy. *Biomaterials* 2011, **32**, 2938-2952.
4 Laurent, S.; Forge, D.; Port, M.; Roch, A.; Robic, C.; Elst, L. Vander; Muller, R. N. Magnetic Iron Oxide Nanoparticles: Synthesis, Stabilization, Vectorization, Physicochemical Characterizations, and Biological Applications. *Chem Rev* 2008, **108**, 2064-2110.
5 Alexiou, C.; Arnold, W.; Klein, R. J.; Parak, F. G.; Hulin, P.; Bergemann, C.; Erhardt, W.; Wagenpfeil, S.; Lübbe, A. S. Locoregional Cancer Treatment with Magnetic Drug Targeting. *Cancer Res* 2000, **60**, 6641-6648.
6 Jordan, A.; Scholz, R.; Wust, P.; Fähling, H.; Felix, R. Magnetic Fluid Hyperthermia (MFH): Cancer Treatment with AC Magnetic Field Induced Excitation of Biocompatible Superparamagnetic Nanoparticles. *J Magn Magn Mater* 1999, **201**, 413-419.
7 Weissleder, R.; Nahrendorf, M.; Pittet, M. J. Imaging Macrophages with Nanoparticles. *Nat Mater* 2014, **13**, 125-138.
8 Crichton, R. Intracellular Iron Metabolism and Cellular Iron Homeostasis. In Inorganic Biochemistry of Iron Metabolism. John Wiley & Sons, Ltd, 2002; pp. 167-190.
9 Crichton, R. Intracellular Iron Storage and Biomineralization. In Inorganic Biochemistry of Iron Metabolism. John Wiley & Sons, Ltd, 2002; pp. 133–165.
10 Balakumaran, A.; Pawelczyk, E.; Ren, J.; Sworder, B.; Chaudhry, A.; Sabatino, M.; Stroncek, D.; Frank, J. A.; Robey, P. G. Superparamagnetic Iron Oxide Nanoparticles Labeling of Bone Marrow Stromal (Mesenchymal) Cells Does Not Affect Their "Stemness." *PLoS One* 2010, **5**, 1-8.
11 Geppert, M.; Hohnholt, M. C.; Nürnberger, S.; Dringen, R. Ferritin up-Regulation and Transient ROS Production in Cultured Brain Astrocytes after Loading with Iron Oxide Nanoparticles. *Acta Biomater* 2012, **8**, 3832-3839.
12 Hohnholt, M. C.; Geppert, M.; Dringen, R. Treatment with Iron Oxide Nanoparticles Induces Ferritin Synthesis but Not Oxidative Stress in Oligodendroglial Cells. *Acta Biomater* 2011, **7**, 3946-3954.
13 Gu, J.; Xu, H.; Han, Y.; Dai, W.; Hao, W.; Wang, C.; Gu, N.; Xu, H.; Cao, J. The Internalization Pathway, Metabolic Fate and Biological Effect of Superparamagnetic Iron Oxide Nanoparticles in the Macrophage-like RAW264.7 Cell. *Sci China Life Sci* 2011, **54**, 793-805.
14 Rojas, J. M.; Sanz-Ortega, L.; Mulens-Arias, V.; Gutiérrez, L.; Pérez-Yagüe, S.; Barber, D. F. Superparamagnetic Iron Oxide Nanoparticle Uptake Alters M2 Macrophage Phenotype, Iron Metabolism, Migration and Invasion. *Nanomed Nanotech Biol Med* 2016, **12**, 1127-1138.
15 Mulens-Arias, V.; Rojas, J. M.; Pérez-Yagüe, S.; Morales, M. P.; Barber, D. F. Polyethylenimine-Coated SPIONs Trigger Macrophage Activation through TLR-4 Signaling and ROS

View Article Online
DOI: 10.1039/C7NR06020C

Production and Modulate Podosome Dynamics. *Biomaterials* 2015, **52**, 494-506.
16 Mazuel, F.; Espinosa, A.; Luciani, N.; Reffay, M.; Le Borgne, R.; Motte, L.; Desboeufs, K.; Michel, A.; Pellegrino, T.; Lalatonne, Y.; et al. Massive Intracellular Biodegradation of Iron Oxide Nanoparticles Evidenced Magnetically at Single-Endosome and Tissue Levels. *ACS Nano* 2016, **10**, 7627-7638.
17 Rojas, J. M.; Gavilán, H.; del Dedo, V.; Lorente-Sorolla, E.; Sanz-Ortega, L.; da Silva, G. B.; Costo, R.; Perez-Yagüe, S.; Talelli, M.; Marciello, M.; et al. Time-Course Assessment of the Aggregation and Metabolization of Magnetic Nanoparticles. *Acta Biomater* 2017, **58**, 181-195.
18 Ruiz, A.; Gutierrez, L.; Cáceres-Velez, P.; Santos, D.; Chaves, S.; Fascineli, M. L.; Garcia, M. P.; Azevedo, R. B.; Morales, M. P. Biotransformation of Magnetic Nanoparticles as a Function of the Coating in a Rat Model. *Nanoscale* 2015, **7**, 16321-16329.
19 James-Zorn, C.; Ponferrada, V. G.; Burns, K. A.; Fortriede, J. D.; Lotay, V. S.; Liu, Y.; Brad Karpinka, J.; Karimi, K.; Zorn, A. M.; Vize, P. D. Xenbase: Core Features, Data Acquisition, and Data Processing. *Genesis* 2015, **53**, 486-497.
20 Nations, S.; Wages, M.; Cañas, J. E.; Maul, J.; Theodorakis, C.; Cobb, G. P. Acute Effects of Fe_2O_3, TiO_2, ZnO and CuO Nanomaterials on Xenopus Laevis. *Chemosphere* 2011, **83**, 1053-1061.
21 Nations, S.; Long, M.; Wages, M.; Canas, J.; Maul, J. D.; Theodorakis, C.; Cobb, G. P. Effects of ZnO Nanomaterials on Xenopus Laevis Growth and Development. *Ecotoxicol Environ Saf* 2011, **74**, 203-210.
22 Webster, C.; Di Silvio, D.; Devarajan, A.; Bigini, P.; Micotti, E.; Giudice, C.; Salmona, M.; Wheeler, G. N.; Sherwood, V.; Baldelli Bombelli, F. An Early Developmental Vertebrate Model for Nanomaterial Safety: Bridging Cell-Based and Mammalian Toxicity Assessment. *Nanomedicine* 2016, **11**, 643-656.
23 Giannaccini, M.; Giannini, M.; Calatayud, M. P.; Goya, G. F.; Cuschieri, A.; Dente, L.; Raffa, V. Magnetic Nanoparticles as Intraocular Drug Delivery System to Target Retinal Pigmented Epithelium (RPE). *Int J Mol Sci* 2014, **15**, 1590-1605.
24 Gutierrez, L.; Costo, R.; Gruttner, C.; Westphal, F.; Gehrke, N.; Heinke, D.; Fornara, A.; Pankhurst, Q. A.; Johansson, C.; Veintemillas-Verdaguer, S.; et al. Synthesis Methods to Prepare Single- and Multi-Core Iron Oxide Nanoparticles for Biomedical Applications. *Dalton Trans* 2015, **44**, 2943-2952.
25 Silva, A. K. A.; Espinosa, A.; Kolosnjaj-Tabi, J.; Wilhelm, C.; Gazeau, F. Medical Applications of Iron Oxide Nanoparticles. In Iron Oxides; Wiley-VCH Verlag GmbH & Co. KGaA, 2016; pp. 425-472.
26 Torchilin, V. Tumor Delivery of Macromolecular Drugs Based on the EPR Effect. *Adv Drug Deliv Rev* 2011, **63**, 131-135.
27 Dutz, S.; Kettering, M.; Hilger, I.; Müller, R.; Zeisberger, M. Magnetic Multicore Nanoparticles for Hyperthermia-influence of Particle Immobilization in Tumour Tissue on Magnetic Properties. *Nanotechnology* 2011, **22**, 265102.
28 Kolosnjaj-Tabi, J.; Lartigue, L.; Javed, Y.; Luciani, N.; Pellegrino, T.; Wilhelm, C.; Alloyeau, D.; Gazeau, F. Biotransformations of Magnetic Nanoparticles in the Body. *Nano Today* 2016, **11**, 280-284.
29 Lázaro, F. J.; Gutiérrez, L.; Abadía, A. R.; Romero, M. S.; López, A. Biological Tissue Magnetism in the Frame of Iron Overload Diseases. *J Magn Magn Mater* 2007, **316**, 126-131.
30 Gutierrez, L.; Abadia, A. R.; Romero, M. S.; Quintana, C.; Morales, M. P.; Patino, C.; Arranz, R. Bioinorganic Transformations of Liver Iron Deposits Observed by Tissue Magnetic Characterisation in a Rat Model. *J Inorg Biochem* 2006, **100**, 1790-1799.
31 Lázaro, F. J.; Gutiérrez, L.; Abadía, A. R.; Romero, M. S.; López, A.; Muñoz, M. J. Whole Tissue AC Susceptibility after Superparamagnetic Iron Oxide Contrast Agent Administration in a Rat Model. *J Magn Magn Mater* 2007, **311**, 460-463.
32 Martin, M.; Rodriguez-Nogales, A.; Garces, V.; Galvez, N.; Gutierrez, L.; Galvez, J.; Rondon, D.; Olivares, M.; Dominguez-Vera, J. M. Magnetic Study on Biodistribution and Biodegradation of Oral Magnetic Nanostructures in the Rat Gastrointestinal Tract. *Nanoscale* 2016, **8**, 15041-15047.
33 Mulvaney, P.; Parak, W. J.; Caruso, F.; Weiss, P. S. Standardizing Nanomaterials. *ACS Nano* 2016, **10**, 9763-9764.
34 Jia, B.; Gao, L. Morphological Transformation of Fe3O4 Spherical Aggregates from Solid to Hollow and Their Self-Assembly under an External Magnetic Field. *J Phys Chem C* 2008, **112**, 666-671.
35 LaConte, L.; Nitin, N.; Bao, G. Magnetic Nanoparticle Probes. *Mater Today* 2005, **8**, 32-38.
36 Mahmoudi, M.; Hofmann, H.; Rothen-Rutishauser, B.; Petri-Fink, A. Assessing the in Vitro and in Vivo Toxicity of Superparamagnetic Iron Oxide Nanoparticles. *Chem Rev* 2012, **112**, 2323-2338.
37 Ruiz, A.; Salas, G.; Calero, M.; Hernández, Y.; Villanueva, A.; Herranz, F.; Veintemillas-Verdaguer, S.; Martínez, E.; Barber, D. F.; Morales, M. P. Short-Chain PEG Molecules Strongly Bound to Magnetic Nanoparticle for MRI Long Circulating Agents. *Acta Biomater* 2013, **9**, 6421-6430.
38 Osborne, O. J.; Lin, S.; Chang, C. H.; Ji, Z.; Yu, X.; Wang, X.; Lin, S.; Xia, T.; Nel, A. E. Organ-Specific and Size-Dependent Ag Nanoparticle Toxicity in Gills and Intestines of Adult Zebrafish. *ACS Nano* 2015, **9**, 9573-9584.
39 Goldstein, J. I.; Newbury, D. E.; Echlin, P.; Joy, D. C.; Romig, A. D.; Lyman, C. E.; Fiori, C.; Lifshin, E. Qualitative X-Ray Analysis. In Scanning Electron Microscopy and X-Ray Microanalysis: A Text for Biologists, Materials Scientists, and Geologists; Springer US: Boston, MA, 1992; pp. 341-364.
40 Yildiz, H. M.; McKelvey, C. A.; Marsac, P. J.; Carrier, R. L. Size Selectivity of Intestinal Mucus to Diffusing Particulates Is Dependent on Surface Chemistry and Exposure to Lipids. *J Drug Target* 2015, **23**, 768-774.
41 Xie, J.; Xu, C.; Kohler, N.; Hou, Y.; Sun, S. Controlled PEGylation of Monodisperse Fe3O4 Nanoparticles for Reduced Non-Specific Uptake by Macrophage Cells. *Adv Mater* 2007, **19**, 3163-3166.
42 Hanini, A.; Schmitt, A.; Kacem, K.; Chau, F.; Ammar, S.; Gavard, J. Evaluation of Iron Oxide Nanoparticle Biocompatibility. *Int J Nanomedicine* 2011, **6**, 787-794.
43 Waldvogel-Abramowski, S.; Waeber, G.; Gassner, C.; Buser, A.; Frey, B. M.; Favrat, B.; Tissot, J.-D. Physiology of Iron Metabolism. *Transfus Med Hemother* 2014, **41**, 213-221.
44 Elgrabli, D.; Dachraoui, W.; De Marmier, H.; Ménard-Moyon, C.; Bégin, D.; Bégin-Colin, S.; Bianco, A.; Alloyeau, D.; Gazeau, F. Intracellular Degradation of Functionalized Carbon Nanotube / Iron Oxide Hybrids Is Modulated by Iron via Nrf2 Pathway. *Sci Rep* 2017, **7**, 40997.
45 Eisenstein, R. S.; Munro, H. N. Translational Regulation of Ferritin Synthesis by Iron. *Enzyme* 1990, **44**, 42-58.
46 Balas, M. R.; Din Popescu, I. M.; Hermenean, A.; Cinteză, O. L.; Burlacu, R.; Ardelean, A.; Dinischiotu, A. Exposure to Iron Oxide Nanoparticles Coated with Phospholipid-Based Polymeric Micelles Induces Biochemical and Histopathological Pulmonary Changes in Mice. *Int J Mol Sci* 2015, **16**, 29417-29435.
47 Mejías, R.; Gutiérrez, L.; Salas, G.; Pérez-Yagüe, S.; Zotes, T. M.; Lázaro, F. J.; Morales, M. P.; Barber, D. F. Long Term Biotransformation and Toxicity of Dimercaptosuccinic Acid-Coated Magnetic Nanoparticles Support Their Use in

View Article Online
DOI: 10.1039/C7NR06020C

Biomedical Applications. *J Control Release* 2013, **171**, 225-233.

48 Mazuel, F; Espinosa, A; Radtke, G; Bugnet, M; Neveu, S; Lalatonne, Y; Botton, GA; Abou-Hassan, A; Wilhelm, C. Magneto-Thermal Metrics Can Mirror the Long-Term Intracellular Fate of Magneto-Plasmonic Nanohybrids and Reveal the Remarkable Shielding Effect of Gold. *Adv Funct Mater* 2017, **27**, 1605997.

49 Salas, G.; Casado, C.; Teran, F. J.; Miranda, R.; Serna, C. J.; Morales, M. P. Controlled Synthesis of Uniform Magnetite Nanocrystals with High-Quality Properties for Biomedical Applications. *J Mater Chem* 2012, **22**, 21065.

50 Sun, Q.; Ren, Z.; Wang, R.; Chen, W.; Chen, C. Magnetite Hollow Spheres: Solution Synthesis, Phase Formation and Magnetic Property. *J Nanoparticle Res* 2011, **13**, 213-220.

51 Jun, Y.; Huh, Y.-M.; Choi, J.; Lee, J.-H.; Song, H.-T.; KimKim; Yoon, S.; Kim, K.-S.; Shin, J.-S.; Suh, J.-S.; et al. Nanoscale Size Effect of Magnetic Nanocrystals and Their Utilization for Cancer Diagnosis via Magnetic Resonance Imaging. *J Am Chem Soc* 2005, **127**, 5732-5733.

52 Martina, M.-S.; Fortin, J.-P.; Ménager, C.; Clément, O.; Barratt, G.; Grabielle-Madelmont, C.; Gazeau, F.; Cabuil, V.; Lesieur, S. Generation of Superparamagnetic Liposomes Revealed as Highly Efficient MRI Contrast Agents for in Vivo Imaging. *J Am Chem Soc* 2005, **127**, 10676-10685.

53 Glahn, R. P.; Lee, O. A.; Yeung, A.; Goldman, M. I.; Miller, D. D. Caco-2 Cell Ferritin Formation Predicts Nonradiolabeled Food Iron Availability in an In Vitro Digestion/Caco-2 Cell Culture Model. *J Nutr* 1998, **128**, 1555-1561.

54 Tomlinson, M. L.; Hendry, A. E.; Wheeler, G. N. Chemical Genetics and Drug Discovery in Xenopus. Xenopus Protocols: Post-Genomic Approaches; HOPPLER, S.; Vize, P. D., Eds.; Humana Press: Totowa, NJ, 2012, 155-166.

55 Mamusa, M.; Sitia, L.; Barbero, F.; Ruyra, A.; Calvo, T. D.; Montis, C.; Gonzalez-Paredes, A.; Wheeler, G. N.; Morris, C. J.; McArthur, M.; et al. Cationic Liposomal Vectors Incorporating a Bolaamphiphile for Oligonucleotide Antimicrobials. *Biochim Biophys Acta- Biomembr* 2017, **1859**, 1767-1777.